Substantial aircraft contrail formation at low soot emission levels

Christiane Voigt

Christiane.Voigt@dlr.de

DLR https://orcid.org/0000-0001-8925-7731

Raphael Märkl

DLR

Daniel Sauer

DLR https://orcid.org/0000-0002-0317-5063

Rebecca Dischl

DLR

Stefan Kaufmann

DLR

Tiziana Bräuer

DLR

Tina Jurkat

DLR

Charles Renard

Airbus

Katharina Seeliger

Airbus

Gauthier Le Chenadec

Airbus

Julien Moreau

Airbus

Fangqun Yu

University at Albany, State University of New York https://orcid.org/0000-0001-8862-4835

Nicolas Bonne

ONERA

Amandine Roche

Safran

Joseph Zelina

GE Aerospace

Andreas Dörnbrack

Deutsches Zentrum für Luft- und Raumfahrt
Lisa Eirenschmalz
DLR
Christopher Heckl
DLR
Elisabeth Horst
DLR
Michael Lichtenstern
German Aerospace Center (DLR), Institute of Atmospheric Physics
Andreas Marsing
https://orcid.org/0000-0002-5006-2133
Anke Roiger
German Aerospace Center (DLR), Institute of Atmospheric Physics
Monika Scheibe
DLR https://orcid.org/0000-0001-8509-1252
Paul Stock
DLR
Andreas Giez
German Aerospace Center (DLR) https://orcid.org/0000-0002-8595-8343
Georg Eckel
DLR
Gregor Neumann
DLR
Margaux Vals
ONERA
Emiliano Requena-Esteban
Airbus
Patrick Le Clercq
DLR https://orcid.org/0000-0001-6011-5625

Physical Sciences - Article

Keywords:

Posted Date: May 9th, 2025

DOI: https://doi.org/10.21203/rs.3.rs-6559440/v1

Additional Declarations: Yes there is potential Competing Interest. CR, KS, GLC, JM and ERE are employed by Airbus, JZ is employed by General Electric, AR is employed by CFM Safran. All other authors declare that they have no conflict of interest.

Demonstration of contrail ice formation from volatile particles on a modern lean-burn combustor engine

Substantial aircraft contrail formation at low soot emission levels

Christiane Voigt[1,2,*], Raphael Märkl[1,2], Daniel Sauer[1], Rebecca Dischl[1,2], Stefan Kaufmann[1], Tiziana Bräuer[1], Tina Jurkat-Witschas[1], Charles Renard[3], Katharina Seeliger[3], Gauthier Le Chenadec[3], Julien Moreau[3], Emiliano Requena-Esteban[3], Fangqun Yu[4], Nicolas Bonne[5], Margaux Vals[5], Amandine Roche[6], Joseph Zelina[7], Andreas Dörnbrack[1], Lisa Eirenschmalz[1], Christopher Heckl[1], Elisabeth Horst[1], Michael Lichtenstern[1], Andreas Marsing[1], Gregor Neumann[1], Anke Roiger[1], Monika Scheibe[1], Paul Stock[1], Andreas Giez[1], Georg Eckel[1], Patrick Le Clercq[1]

[1]Deutsches Zentrum für Luft- und Raumfahrt (DLR), Oberpfaffenhofen, Germany

[2]Johannes Gutenberg-University, Mainz, Germany

[3]Airbus Operations SAS, Toulouse, France

[4]Atmospheric Sciences Research Center, University Albany, United States

[5]Office National d'Etudes et de Recherches Aérospatiales (ONERA), Palaiseau, France

[6]Safran Aircraft Engines, Villaroche, France

[7]GE Aerospace, Cicinnati, Ohio, United States

*corresponding author: Christiane.Voigt@dlr.de

Abstract

Contrail cirrus are a major contributor to the climate forcing from aviation. Yet, the number of contrail ice crystals forming behind aircraft with modern lean-burn engines is unknown. Theory spans a five orders of magnitude range in ice crystal numbers – rendering related climate effects unpredictable. Here, we present first in-flight observations of contrails formed behind an aircraft with lean-burn engine technology. We find a massive reduction in soot particle number emissions, three orders of magnitude lower than soot emissions from conventional rich-quench-lean engines. In contrast, volatile particle number emissions - as well as contrail ice crystal numbers - exceed 10^{15} particles per kilogram of burned fuel. We provide first experimental evidence and theoretical explanations for contrail ice activation on volatile aerosol in the absence of soot. Our results demonstrate the impact of lean-burn engine configurations, fuel composition, and ambient conditions on contrail ice crystal numbers. The integration of our data in models will enable to reliably predict the fleet-wide contrail climate effect. Our findings point to the need to minimize volatile particle emissions and affect industrial decisions on engine and fleet design for competitive and clean future aviation.

Aviation plays a vital role for mankind, industry, and economy and the transport of goods and people. Aircraft also contribute to climate change mainly by carbon dioxide emissions and by formation of contrail cirrus. Notably, the annual mean effective radiative forcing (ERF) from contrails is about on par with that from aviation's carbon dioxide emissions since the historical start of air traffic (Burkhardt et al., 2018; Lee et al., 2021). Meanwhile, global air traffic has recovered from the 2020 pandemic (Schumann et al., 2021) and is expected to increase by a factor of two to three by 2050 (Bock and Burkhardt, 2019; Grewe et al., 2021). Hence, there is the urgent need for an international aviation strategy that reflects the essential role of aviation for economy and global competitiveness - and which also curbs aircraft emissions, contrails, and related climate effects (Arrowsmith, 2020; Dray et al., 2022). This is also expressed in environmental efforts by the International Civil Aviation Organization (ICAO, 2024) and the general commitment to fly net-zero carbon emissions by 2050 signed by 16 major players in the aviation sector (ATAG, 2025). Regulators have reacted to this aviation challenge, and the European Union has released the Destination 2050 Roadmap (EU, 2025a), which sets limits on aircraft CO_2 emissions and the ReFuelEU initiative to support the ramp up of the production of Sustainable Aviation Fuels (SAF). Finally, on top of the Emission Trading System (ETS, Pechstein, 2017) for CO_2, and the international Carbon Offsetting and Reduction Scheme for International Aviation (CORSIA, ICAO, 2023), the European Commission demands the monitoring and reporting of aviation's non-CO_2 effects starting from 2025 (EU, 2025b). This programme will enable regulations for the aviation industry to reduce non-CO_2 effects such as contrails and NO_x. Parallel to a debate on uncertainty (Lee et al., 2021) or the best suited metric (e.g. Megill et al., 2024), academia and industry have made considerable progress to better understand aviation's non-CO_2 effects and to develop advanced solutions to reduce the total climate effect from aviation. Current options include alternative bio-based or synthetic fuels (Moore et al., 2017; Voigt et al., 2021; Bergero et al., 2023), engine and aircraft technology (Kaufmann et al., 2024) as well as operational measures (Sonabend et al., 2025).

Unlike well-mixed carbon dioxide emissions with atmospheric lifetimes of many decades (IPCC 2023), contrail cirrus may persist at cold and humid cruise conditions for only several hours (Minnis et al., 1998; Vazquez-Navarro et al., 2015; Wang et al., 2023). Hence, unlike CO_2, measures to reduce warming contrail cirrus would have an immediate effect on the climate, which is one of the levers required to meet the international climate targets.

Current contrail mitigation strategies include avoiding the formation of contrails by flying above or below ice supersaturated regions where warming contrails would form (Teoh et al., 2024, Wang et al., 2025). While these operational measures may come at the cost of slightly increased fuel consumption (Martin-Frias et al., 2024), it has been found that a potential climate gain can be achieved independent of the selected metrics (Borella et al., 2024) and at low operational costs for individual flights (Simorg and Soler, 2025; Sonabend et al., 2024).

Another promising strategy to reduce the contrail climate effect are bio-based or synthetic aviation fuels produced with renewable energies which have a significantly reduced CO_2 footprint compared to conventional Jet A-1 (Jing et al., 2022). Due to their lower aromatic fuel content, SAFs lead to a reduction in soot particle emissions (Beyersdorf et al., 2014; Moore et al., 2017; Dischl et al., 2024). For conventional rich-quench-lean (RQL) engine technologies, the soot particles in the size range around 30 nanometres serve as primary nuclei for contrail ice crystals (Kleine et al., 2018; Heymsfield et al., 2010) and a significant reduction in soot and contrail ice crystals has been observed when burning low aromatic SAF (Voigt et al., 2021; Bräuer et al., 2021; Märkl et al., 2024). This can reduce the lifetime of contrails (Teoh et al., 2022a), and their radiative forcing (Burkhardt et al., 2018; Märkl et al., 2024).

While the effects of SAF on contrails and climate have been investigated RQL combustor technologies, in-flight emissions and contrail data from modern lean-burn combustors are missing, which leads to uncertainties in current contrail climate impact predictions. Lean-burn engines are designed to improve engine emission performance via a fuel injection system and an airflow distribution that expands regions with a low fuel-to air ratios in the combustor. This results in lower nitrogen oxides, and soot particle emissions (Stickles and Barret, 2013). Emission certification tests with lean-burn engines also indicate very low soot mass and number emissions at higher power settings (ICAO, 2025).

Models (Kärcher and Yu, 2009; Rojo et al., 2015; Kärcher, 2018; Jones and Miake-Lye, 2023; Yu et al., 2024) predict a near-linear dependence between emitted soot particles and contrail ice crystal numbers for current RQL engines. A completely different behaviour is predicted in the low-soot regime ($<<10^{14}$ soot particles emitted per kg of fuel burned) eventually expected for lean-burn engines. Here, microphysical contrail models suggest a large range in ice crystal numbers covering four orders of magnitude variations, which lack experimental evidence. In

particular, there are no published particle number emission data for lean-burn engines at cruise. Finally, there is also a complete gap of contrail data from lean-burn engines, required to calculate the related climate effects.

As data are missing, most climate models (Bier et al., 2022; Gettelman et al., 2021) as well as lightweight climate response models (e.g. Arriolabengoa et al., 2024) assume very low initial ice crystal numbers for lean-burn aircraft - potentially underestimating the related contrail climate effects. This gap propagates into future fleet simulations (Grewe et al., 2021; Brazzola et al., 2025), possibly with unreliable predictions for hydrogen-based technologies (Dray et al., 2022).

In-flight emission and contrail measurements with lean-burn engine technology

Here, we provide the first in-flight data set on engine emissions and contrail properties produced by an aircraft with lean-burn engines. During the NEOFUELS/VOLCAN (VOL avec Carburants Alternatif Nouveaux) campaign, the Deutsches Zentrum für Luft- und Raumfahrt (DLR) partnered with the aircraft manufacturer Airbus and the engine manufacturer SAFRAN to measure the emissions of an A321neo equipped with state-of-the-art LEAP-1A engines by CFM/SAFRAN. Under normal operation, the combustor of the LEAP-1A engine is staged to the lean-burn mode at high power settings during take-off, climb and cruise phases. There, the inner pilot and the outer main fuel injectors are active, while during descent at low power, the outer injector is switched off to guarantee stable combustion in a kind of rich-burn mode. Engine control adjustments were developed by the engine manufacturer specifically for this campaign to overwrite the normal fuel injector control law in the automated engine control (FADEC) and allow for defined operation either in controlled lean-burn or in forced rich-burn combustion mode at the same combustor inlet temperature.

The fuel system of the A321neo has three separate tanks which can be switched to the different engines independently and enabled testing of different fuels during the same flight. The A321neo was fueled with conventional petroleum-based fossil kerosene as well as 100% bio-based hydrotreated ester and fatty acids synthetic paraffinic kerosene (HEFA-SPK), with different hydrogen, aromatic, naphthalene, and sulfur compositions, both provided by Total Energies. The aircraft and the engines were specifically cleared for operations with 100% HEFA-SPK and the composition and properties of investigated fuels are given in Table 1.

The DLR research aircraft Falcon 20E (Voigt et al., 2011) was equipped with a comprehensive set of instruments to measure trace gases, in particular carbon dioxide, water vapor, and nitrogen oxides, as well as properties of aerosol and contrail ice particles, and meteorological data, as described in detail in the methods section. The Falcon chased the A321neo at close distances between 30 to 160 m during repeated emission measurements of the right engine in different engine modes and for different fuels (Figure 1a). As contrail ice crystal formation can be incomplete at less than 1 second plume age, contrails were probed in the far field in 6 to 29 km distance to the preceding aircraft in traffic restricted airspaces over the Atlantic and the Mediterranean. After the flights, the particle emission and contrail data were dilution-corrected and correlated to the fuel consumption. Detailed information on the aircraft, engines, instrumentation, data evaluation and models is provided in the methods section.

Results – Aerosol and contrail ice particle numbers in forced rich-burn and lean-burn combustion modes

The particle number emission index (EI_x) measures the number of non-volatile or total particles emitted per kilogram of burned fuel assuming that the fuel carbon content is completely converted to CO_2, see also methods. We measured a median non-volatile particle number emission index EI_{nv} in the forced rich-burn mode of the LEAP-1A engine on the A321neo of 1.0×10^{15} (range: 0.8 to 1.1×10^{15}) particles per kilogram-fuel burned for the fossil petroleum-based Jet A-1 fuel probed during the campaign (Figure 1, Table 2). While forcing the combustor to operate in rich-burn mode does not reflect the typical and optimal combustor setting at cruise, it is used here to compare rich-burn and lean-burn engine emissions at similar power settings in terms of combustor inlet temperature T30. The measured EI_{nv} is lower compared to data from older engines with higher soot emissions of the IAE V2500 family (Voigt et al., 2021; Bräuer et al., 2021). It is slightly higher compared to cruise data from a modern Rolls-Royce Trent XWB-84 engine (Dischl et al., 2024) or an engine of the CFM56 family (Moore et al., 2017) measured at different ambient and engine conditions.

Particle number emission indices were also measured in the lean-burn combustion mode of the LEAP-1A engine on the A321neo. Here, the EI_{nv} is massively reduced by three orders of magnitude to a median of 1.0×10^{12} (range from 0.5 to 1.9×10^{12}) kg^{-1}-fuel. These are the first in-flight emission data from lean-burn engines at cruise. The EI_{nv} is slightly above the detection

limit determined by the ambient aerosol background concentration plus three times its standard deviation. The reduction in soot particle numbers of the LEAP-1A in typical lean-burn cruise conditions is large. As soot particles are the preferred nuclei for contrail ice crystals (Kärcher and Yu, 2009), the question arises whether ice crystal numbers in contrails are reduced by the same order of magnitude.

To this end, contrail measurements were carried out with both engines operating in the typical lean-burn cruise mode. Persistent contrails were detected at 5 to 40 km distance behind the preceding A321neo in ice supersaturated conditions, see also Table 3. The apparent contrail ice particle number emission index EI_{ice} is calculated analogously to EI_{nv}. For the contrails detected under lean-burn conditions, mean EI_{ice} ranged between 0.06 and 2 $\times 10^{15}$ ice particles kg^{-1}-fuel. Variability in ambient conditions, fast non-equilibrium ice nucleation processes on emitted aerosols, and different fuel compositions contribute to the large range in EI_{ice}. Summarized, EI_{nv} is three orders of magnitude lower than EI_{ice} and cannot explain the observed high ice particle concentrations.

To explore other potential ice nuclei, we direct the attention to the total particle number emission index EI_t, including non-volatile and volatile particles with diameters larger than 5 nm measured in the near-field in lean-burn conditions (Figure 1). For Jet A-1, EI_t has a median value of 2.1×10^{15} kg^{-1}-fuel and a range of 2.0 to 3.3×10^{15} kg^{-1}-fuel. Similar EI_t are measured in the rich-burn regime promoting the question whether these volatile particles could play a role for contrail ice formation at very low engine soot emission levels.

Contrail formation for lean-burn engines

To assess the role of non-soot particles as potential contrail ice nuclei, two contrail models (Rojo et al., 2015; Yu et al., 2024) were further developed. In addition to non-volatile soot particles, the models calculate the nucleation of volatile aerosol, including ion-induced sulfate aerosol, organic aerosol from unburnt fuel components, and their role in contrail ice formation. In addition, also nucleation (Rojo et al., 2015) or condensation (Yu et al., 2024) of organic vapors stemming from venting of lubrication oils into the exhaust plume (Ungeheuer et al., 2022) are simulated. Both models consider the condensation of gaseous species onto volatile aerosol and/or soot and the competition in gas uptake by larger emitted soot or smaller newly formed volatile aerosols. Differences in the specific model setup are given in the methods.

For sulfur-rich fuels and cold temperatures, both models show that newly formed volatile sulfate, organic and lubrication oil particles sufficiently explain measured contrail ice crystal numbers in the low-soot regime (Figure 2). The results also point to a strong dependence of contrail ice crystal numbers in the lean-burn regime on the fuel sulfur content with EI ranging from 195 (below world average) to 3 (low-sulfur fuel) mg kg^{-1}-fuel. Sulfur-rich fuels tend to produce higher numbers of sulfate aerosol particles which can act as ice nuclei at lowest soot emission levels. Further, the temperature dependent activation of the volatile organo-sulfate particles is evident (Figure 2 a and c). At cold temperatures, the maximum water supersaturation ratio in the plume is high which enables the activation of more small volatile particles into ice crystals.

However, high ice crystal numbers were also measured for HEFA fuels with low sulfur and organic contents. Organics from unburned fuel components or from venting of lubrication oil vapors in the center core of the engine exhaust suggest additional ice nucleation pathways potentially from newly formed organic and/or lubrication oil particles or by condensational growth of the low volatile vapors onto the existing aerosols. While the two models generally capture the measured trends in contrail ice crystal numbers in the low soot regime, they tend to slightly underestimate EI_{ice} at low sulfur and low organic levels at cold temperatures.

In contrast, in the soot-rich regime we observe a correlation of EI_{nv} and EI_{ice} in the forced rich-burn combustion mode, confirming previous observations from RQL engines (Voigt et al., 2021; Bräuer et al., 2021; Märkl et al., 2024). EI_{ice} shown here were measured in a wider temperature and humidity range compared to previous campaigns, which leads to the larger spread in measured EI_{ice} in Figure 2 and 3. Our findings confirm the expectations that soot particles largely regulate the number of contrail ice crystals in the high-soot regime (>10^{14} soot particles kg^{-1}-fuel), and that temperature and low volatile aerosols can influence this trend.

More evidence for contrail ice formation on total (i.e. volatile and soot) aerosol is found when plotting EI_{ice} versus EI_t, the emission index of total aerosol measured in the less than two sec-old exhaust for rich-burn and lean-burn combustor conditions, see Figure 3. EI_t is in the range of 0.4 to 3×10^{15} kg^{-1} for both regimesand the different fuels probed. Also, EI_t is almost linearly correlated with EI_{ice}, and encompassed by the 1:1 and 0.1:1 line. Lowest EI_t of 4×10^{14} kg^{-1} suggest that ice nucleation on ambient aerosol plays a minor role for current engine generations at the ambient conditions where measurements were taken. Generally, total aerosols, i.e. volatiles

and soot, contribute to contrail ice formation in both engine modes. In the rich-burn regime, EI_t and EI_{ice} are dominated by soot particle emissions, while in the soot-poor lean-burn regime, EI_t and EI_{ice} are dominated by newly formed volatile organo-sulfate aerosols facilitated by condensation of lubrication oil vapors. The intermediate regime depends on many parameters and includes the point with a minimum contrail ice crystal number, which still needs to be explored.

The ice nucleation theory for RQL and lean-burn engines is sketched in Figure 4. In the high-soot regime of current RQL engines, ice preferentially nucleates on the larger soot particles emitted by RQL combustors. The emitted soot particles are activated by sulfuric acid to form liquid droplets that are efficient ice nuclei. In the almost complete absence of soot particles in the lean-burn regime (lower part of Figure 4), ice nucleates preferentially on newly formed volatile aerosols. Ions emitted by the engines and low volatile gaseous species form volatile sulfate and organic aerosols (Yu and Turco, 1997; Wong and Miake-Lye, 2010; Rojo et al., 2015). Lubrication oil vapors (Fushimi et al., 2019; Ungeheuer et al., 2022; Ponsonby et al., 2024) condense on preexisting aerosol or form new particles, which can act as ice nuclei. This results in similar ranges of contrail ice crystal number concentrations for aircraft with lean-burn or RQL engines, respectively. Thus, contrail ice numbers can be modified by changes in the fuel composition (sulfur, hydrogen, aromatic, and naphthalene content) and might be affected by the oil venting system. Further experiments are required to better assess the dependence of aerosol and contrail formation on fuel composition for specific engines.

Implications for fuel and engine design, modeling and regulations

Our in-flight observations behind an aircraft with lean-burn engines show substantial volatile aerosol and contrail ice particle formation in the low-soot regime. Therefore, in addition to current ICAO regulations for new engines to monitor non-volatile particle number and mass emissions in the landing and take-off cycle, actions to minimize and monitor volatile particle emissions are required to progress towards clean aviation.

The formation of a few very large oil droplets has been reported from ground emission measurements behind RQL engines with an oil venting system in the colder bypass flow (Linke-Deisinger, 2008; Moore et al., 2015). In contrast, the venting of lubrication oil into hot areas of the core exhaust can lead to the formation of oil vapors, which then recondense on existing

aerosol or nucleate new particles. Both processes can enhance contrail ice particle concentrations. Additional experiments with targeted instrumentations on the ground (e.g. Moore et al., 2017b) and in-flight are needed to explore whether oil emissions are a significant driver for contrail ice formation in the low-soot regime at cruise. Nevertheless, our results give data-driven information to engine manufacturers for the design of the oil venting system as a lever to reduce total particle emissions.

More experiments are required to investigate contrail formation with sulfur-free fuel in order to test whether sulfur-free fuels could reduce contrail ice crystal numbers in the lean-burn mode. First indications were found for RQL combustors, that low-sulfur fuels might reduce soot particle activation and thereby contrail ice crystals (Wong and Miake-Lye, 2010; Voigt et al., 2021; Jones and Miake-Lye, 2023; Märkl et al., 2024; Yu et al., 2024). Also, engine-to-engine variability and effects of engine deterioration on emissions need to be explored to assess emissions at cruise.

Results of this work need to be implemented in global fleet models. Currently about 6% of passenger flights globally are operated by lean-burning engines, and the trend is increasing (Teoh et al., 2024). Assumptions of low contrail ice crystal numbers by lean-burn engines can underestimate their climate impact (e.g. Bier et al., 2022; Teoh et al., 2024) and observation-based model updates including data on microphysical and radiative contrail properties, atmospheric conditions are required to derive reliable contrail climate forcing predictions. Our results also highlight the importance of reliable assumptions on volatile and non-volatile particle emissions when assessing pathways for climate neutral aviation, including hydrogen-based technologies (Dray et al., 2022; Arriolabengoa et al., 2024). Summarized, our findings provide evidence for the design of next-generation engines and fuels to progress towards clean and competitive future aviation.

References

Arriolabengoa, S., Planès, T., Mattei, P. et al. Lightweight climate models could be useful for assessing aviation mitigation strategies and moving beyond the CO_2-equivalence metrics debate. Commun Earth Environ 5, 716, https://doi.org/10.1038/s43247-024-01888-5, 2024.

Arrowsmith, S. Report from the Commission to the European Parliament and the Council: Updated analysis of the non-CO2 climate impacts of aviation and potential policy measures pursuant to EU Emissions Trading System Directive Article 30(4), MOVE/E1/SER/2019-475/SI2.817062,

https://www.easa.europa.eu/sites/default/files/dfu/201119_report_com_ep_council_updated_analysis_non_co2_climate_impacts_aviation.pdf, 2020.

ATAG2025, Aviation Transport Action Group, https://atag.org. last accessed 24032025.

Bergero, C., Gosnell, G., Gielen, D. et al. Pathways to net-zero emissions from aviation. Nature Sustainability 6, 404-414; https://doi.org/10.1038/s41893-022-01046-9, 2023.

Beyersdorf, A. J., Timko, M. T., Ziemba, L. D., Bulzan, D., Corporan, E., Herndon, S. C., Howard, R., Miake-Lye, R., Thornhill, K. L., Winstead, E., Wey, C., Yu, Z., and Anderson, B. E.: Reductions in aircraft particulate emissions due to the use of Fischer–Tropsch fuels, Atmos Chem Phys, 14, 11–23, https://doi.org/10.5194/acp-14-11-2014, 2014.

Bier, A. and Burkhardt, U.: Impact of Parametrizing Microphysical Processes in the Jet and Vortex Phase on Contrail Cirrus Properties and Radiative Forcing, Journal of Geophysical Research: Atmospheres, 127, https://doi.org/10.1029/2022JD036677, 2022.

Bock, L. and Burkhardt, U.: Contrail cirrus radiative forcing for future air traffic, Atmospheric Chemistry and Physics, 19, 8163–8174, https://doi.org/10.5194/acp-19-8163-2019, 2019.

Bräuer, T., Voigt, C., Sauer, D., Kaufmann, S., Hahn, V., Scheibe, M., Schlager, H., Huber, F., Clercq, P. L., Moore, R. H., and Anderson, B. E.: Reduced ice number concentrations in contrails from low-aromatic biofuel blends, Atmos Chem Phys, 21, 16 817–16 826, https://doi.org/10.5194/acp-21-16817-2021, 2021.

Brazzola, N., Meskaldji, A., Patt, A. et al. The role of direct air capture in achieving climate-neutral aviation. Nat Commun 16, 588. https://doi.org/10.1038/s41467-024-55482-6, 2025.

Burkhardt, U., Bock, L., and Bier, A.: Mitigating the contrail cirrus climate impact by reducing aircraft soot number emissions, npj Climate and Atmospheric Science, 1, https://doi.org/10.1038/s41612-018-0046-4, 2018.

Dischl, R., Sauer, D., Voigt, C., Harlaß, T., Sakellariou, F., Märkl, R., Schumann, U., Scheibe, M., Kaufmann, S., Roiger, A., Dörnbrack, A., Renard, C., Gauthier, M., Swann, P., Madden, P., Luff, D., Johnson, M., Ahrens, D., Sallinen, R., Schripp, T., Eckel, G., Bauder, U., and Le Clercq, P.: Measurements of particle emissions of an A350-941 burning 100 % sustainable aviation fuels in cruise, Atmos. Chem. Phys., 24, 11255–11273, https://doi.org/10.5194/acp-24-11255-2024, 2024.

Dray, L., Schäfer, A.W., Grobler, C. et al. Cost and emissions pathways towards net-zero climate impacts in aviation. Nat. Clim. Change 12, 956–962, https://doi.org/10.1038/s41558-022-01485-4, 2022.

Epstein, A. H.: Aeropropulsion for Commercial Aviation in the Twenty-First Century and Research Directions Needed, AIAA Journal, 52, 901–911, https://doi.org/10.2514/1.J052713, 2014.

EU2025a; Destination 2050 pathways for aviation, https://www.destination2050.eu, and ReFuel EU Initiative; https://transport.ec.europa.eu/transport-modes/air/environment/refueleu-aviation_en, last accessed 24032025.

EU2025b, Non-CO_2 Monitoring Reporting and Verification System; https://climate.ec.europa.eu/eu-action/transport/reducing-emissions-aviation_en#documentationlast accessed 04042025.

Fushimi, A., Saitoh, K., Fujitani, Y., and Takegawa, N.: Identification of jet lubrication oil as a major component of aircraft exhaust nanoparticles, Atmospheric Chemistry and Physics, 19, 6389–6399, https://doi.org/10.5194/acp-19-6389-2019, 2019.

Gettelman, A., Chen, C.-C., and Bardeen, C. G.: The climate impact of COVID-19-induced contrail changes, Atmos. Chem. Phys., 21, 9405–9416, https://doi.org/10.5194/acp-21-9405-2021, 2021.

Grewe, V., Rao, A. G., Grönstedt, T., Xisto, C., Linke, F., Melkert, J., Middel, J., Ohlenforst, B., Blakey, S., Christie, S., Matthes, S., and Dahlmann, K.: Evaluating the climate impact of aviation emission scenarios towards the Paris agreement including COVID-19 effects, Nature Comm., 12, https://doi.org/10.1038/s41467-021-24091-y, 2021.

Hadaller, O. J. and Johnson, J. M.: World Fuel Sampling Program, Final Report CRC Report No. 647, Coordinating Research Council, Inc., 2006.

ICAO2023, Carbon Offsetting and Reduction Scheme for International Aviation (CORSIA), https://www.icao.int/environmental-protection/CORSIA, 2023.

ICAO2024, International Civil Aviation Organization fuels guide, https://www.icao.int/environmental-protection/knowledge-sharing/Docs/Sustainable%20Aviation%20Fuels%20Guide_vf.pdf, and non-CO2 conference https://www.icao.int/Meetings/SymposiumNonCO2AviationEmissions2024, 2024.

ICAO2025, engine emission database v30 https://www.easa.europa.eu/en/domains/environment/icao-aircraft-engine-emissions-databank, last accessed 20250324, 2025.

IPCC2023: Climate Change 2023: Synthesis Report. Contribution of Working Groups I, II and III to the Sixth Assessment Report of the Intergovernmental Panel on Climate Change [Core Writing Team, H. Lee and J. Romero (eds.)]. IPCC, Geneva, Switzerland, 35-115, doi:10.59327/IPCC/AR6-9789291691647, 2023.

Jing, L., El-Houjeiri, H.M., Monfort, J. C. et al. Understanding variability in petroleum jet fuel life cycle greenhouse gas emissions to inform aviation decarbonization. Nat Commun 13, 7853, https://doi.org/10.1038/s41467-022-35392-1, 2022.

Jones, S. H. and Miake-Lye, R. C.: Contrail Modeling of ECLIF2/ND-MAX flights: Effects of nvPM Particle Numbers and Fuel Sulfur Content, Meteorologische Zeitschrift, https://doi.org/10.1127/metz/2023/1180, 2023.

Kaufmann S., Dischl, R., and Voigt,C.: Regional and seasonal impact of hydrogen propulsion systems on potential contrail cirrus cover, Atmospheric Environment: X, 24, https://doi.org/10.1016/j.aeaoa.2024.100298, 2024.

Kleine, J., Voigt, C., Sauer, D., Schlager, H., Scheibe, M., Jurkat-Witschas, T., Kaufmann, S., Kärcher, B., and Anderson, B. E.: In Situ Observations of Ice Particle Losses in a Young Persistent Contrail, Geophys Res Lett, 45, 13,553–13,561, https://doi.org/10.1029/2018gl079390, 2018.

Kärcher, B. and Yu, F.: Role of aircraft soot emissions in contrail formation, Geophysical Research Letters, 36, https://doi.org/10.1029/2008GL036649, 2009.

Kärcher, B.: Formation and radiative forcing of contrail cirrus, Nature Commun, 9, https://doi.org/10.1038/s41467-018-04068-0, 2018.

Lee, D., Fahey, D., Skowron, A., Allen, M., Burkhardt, U., Chen, Q., Doherty, S., Freeman, S., Forster, P., Fuglestvedt, J., Gettelman, A., León, R. D., Lim, L., Lund, M., Millar, R., Owen, B., Penner, J., Pitari, G., Prather, M., Sausen, R., and Wilcox, L.: The contribution of global aviation to anthropogenic climate forcing for 2000 to 2018, Atmos Environ, https://doi.org/10.1016/j.atmosenv.2020.117834, 2021.

Linke-Deisinger, Andreas: Systems of Commercial Turbofan Engines: An Introduction to Systems Functions, Springer, ISBN 978-3-540-73618-9, 2008.

Märkl, R. S., Voigt, C., Sauer, D., Dischl, R. K., Kaufmann, S., Harlaß, T., Hahn, V., Roiger, A., Weiß-Rehm, C., Burkhardt, U., Schumann, U., Marsing, A., Scheibe, M., Dörnbrack, A., Renard, C., Gauthier, M., Swann, P., Madden, P., Luff, D., Sallinen, R., Schripp, T., and Le Clercq, P.: Powering aircraft with 100 % sustainable aviation fuel reduces ice crystals in contrails, Atmos. Chem. Phys., 24, 3813–3837, https://doi.org/10.5194/acp-24-3813-2024, 2024.

Megill, L., Deck, K. & Grewe, V.: Alternative climate metrics to the Global Warming Potential are more suitable for assessing aviation non-CO_2 effects. Commun Earth Environ 5, 249, https://doi.org/10.1038/s43247-024-01423-6, 2024.

Minnis, P., Young, D. F., Garber, D. P., Nguyen, L., Smith, W. L., and Palikonda, R.: Transformation of contrails into cirrus during SUCCESS, Geophysical Research Letters, 25, 1157–1160, https://doi.org/10.1029/97GL03314, 1998.

Moore, R. H., Shook, M., Beyersdorf, A., Corr, C., Herndon, S., Knighton, W. B., Miake-Lye, R., Thornhill, K. L., Winstead, E. L., Yu, Z., Ziemba, L. D., and Anderson, B. E.: Influence of Jet Fuel Composition on Aircraft Engine Emissions: A Synthesis of Aerosol Emissions Data from the NASA APEX, AAFEX, and ACCESS Missions, Energy Fuels, 29, 2591–2600, https://doi.org/10.1021/ef502618w, 2015.

Moore, R. H., Thornhill, K. L., Weinzierl, B., Sauer, D., D'Ascoli, E., Kim, J., Lichtenstern, M., Scheibe, M., Beaton, B., Beyersdorf, A. J., Barrick, J., Bulzan, D., Corr, C. A., Crosbie, E., Jurkat, T., Martin, R., Riddick, D., Shook, M., Slover, G., Voigt, C., White, R., Winstead, E., Yasky, R., Ziemba, L. D., Brown, A., Schlager, H., and Anderson, B. E.: Biofuel blending reduces particle emissions from aircraft engines at cruise conditions, Nature, 543, 411–415, https://doi.org/10.1038/nature21420, 2017.

Moore, R., Shook, M., Ziemba, L. et al.: Take-off engine particle emission indices for in-service aircraft at Los Angeles International Airport. Sci Data 4, 170198, https://doi.org/10.1038/sdata.2017.198, 2017b.

Pechstein, J.: European Emissions Trading Scheme, pp. 687–702, Springer Berlin Heidelberg, doi:10.1007/978-3-662-53065-8_26, 2017.

Ponsonby, J., King, L., Murray, B. J., and Stettler, M. E. J.: Jet aircraft lubrication oil droplets as contrail ice-forming particles, Atmos. Chem. Phys., 24, 2045–2058, https://doi.org/10.5194/acp-24-2045-2024, 2024.

Rojo C., Vancassel X., Mirabel P., Ponche J.-L., Garnier F., Impact of alternative jet fuels on aircraft-induced aerosols, Fuel, Volume 144, Pages 335-341, https://doi.org/10.1016/j.fuel.2014.12.021, 2015.

Schumann, U.: On Conditions for Contrail Formation from Aircraft Exhausts, Meteorol Z, 5, 4–23, https://doi.org/10.1127/metz/5/1996/4, 1996.

Schumann, U., Poll, I., Teoh, R., Koelle, R., Spinielli, E., Molloy, J., Koudis, G. S., Baumann, R., Bugliaro, L., Stettler, M., and Voigt, C.: Air traffic and contrail changes over Europe during COVID-19: a model study, Atmos. Chem. Phys., 21, 7429–7450, https://doi.org/10.5194/acp-21-7429-2021, 2021.

Simorgh, A., Soler, M.: Climate-optimized flight planning can effectively reduce the environmental footprint of aviation in Europe at low operational costs. Nat. Commun Earth Environ 6, 66, https://doi.org/10.1038/s43247-025-02031-8, 2025.

Sonabend, A., Elkin, C., Dean, T. et al.: Feasibility test of per-flight contrail avoidance in commercial aviation. Nat. Commun Eng, 3, 184, https://doi.org/10.1038/s44172-024-00329-7, 2024.

Stickles, R., J. Barrett, TAPS II (Twin Annular Premixing Swirler) lean burn combustion system, FAA report number DOT/FAA/AEE/2014-03, https://www.faa.gov/sites/faa.gov/files/about/office_org/headquarters_offices/apl/TAPS_II_Public_Final_Report, 2013.

Teoh, R., Schumann, U., Gryspeerdt, E., Shapiro, M., Molloy, J., Koudis, G., Voigt, C., and Stettler, M. E. J.: Aviation contrail climate effects in the North Atlantic from 2016 to 2021, Atmospheric Chemistry and Physics, 22, 10 919–10 935, https://doi.org/10.5194/acp-22-109192022, 2022a.

Teoh, R., Schumann, U., Voigt, C., Schripp, T., Shapiro, M., Engberg, Z., Molloy, J., Koudis, G., and Stettler, M. E. J.: Targeted Use of Sustainable Aviation Fuel to Maximize Climate Benefits, Environ Sci Technol, 56, 17 246–17 255, https://doi.org/10.1021/acs.est.2c05781, 2022b.

Teoh, R., Engberg, Z., Schumann, U., Voigt, C., Shapiro, M., Rohs, S., and Stettler, M. E. J.: Global aviation contrail climate effects from 2019 to 2021, Atmos. Chem. Phys., 24, 6071–6093, https://doi.org/10.5194/acp-24-6071-2024, 2024.

Ungeheuer, F., Caudillo, L., Ditas, F., Simon, M., van Pinxteren, D., Kılıç, D., Rose, D., Jacobi, S., Kürten, A., Curtius, J., and Vogel, A. L.: Nucleation of jet engine oil vapors is a large source of aviation-related ultrafine particles, Communications Earth and Environment, 3, https://doi.org/10.1038/s43247-022-00653-w, 2022.

Vazquez-Navarro, M., Mannstein, H., and Kox, S.: Contrail life cycle and properties from 1 year of MSG/SEVIRI rapid-scan images, Atmospheric Chemistry and Physics, 15, 8739–8749, https://doi.org/10.5194/acp-15-8739-2015, 2015.

Voigt, C., Schumann, U., Jessberger, P., Jurkat, T., Petzold, A., Gayet, J.-F., Krämer, M., Thornberry, T., and Fahey, D. W.: Extinction and optical depth of contrails, Geophys Res Lett, 38, https://doi.org/10.1029/2011GL047189, 2011.

Voigt, C., Kleine, J., Sauer, D., Moore, R. H., Bräuer, T., Clercq, P. L., Kaufmann, S., Scheibe, M., Jurkat-Witschas, T., Aigner, M., Bauder, U., Boose, Y., Borrmann, S., Crosbie, E., Diskin, G. S., DiGangi, J., Hahn, V., Heckl, C., Huber, F., Nowak, J. B., Rapp, M., Rauch, B., Robinson, C., Schripp, T., Shook, M., Winstead, E., Ziemba, L., Schlager, H., and Anderson, B. E.: Cleaner burning aviation fuels can reduce contrail cloudiness, Communications Earth & Environment, 2, https://doi.org/10.1038/s43247-021-00174-y, 2021.

Wang, Z., Bugliaro, L., Jurkat-Witschas, T., Heller, R., Burkhardt, U., Ziereis, H., Dekoutsidis, G., Wirth, M., Groß, S., Kirschler, S., Kaufmann, S., and Voigt, C.: Observations of microphysical properties and radiative effects of a contrail cirrus outbreak over the North Atlantic, Atmos. Chem. Phys., 23, 1941–1961, https://doi.org/10.5194/acp-23-1941-2023, 2023.

Wang, Z., Bugliaro, L., Gierens, K., Hegglin, M. I., Rohs, S., Petzold, A., Kaufmann, S., and Voigt, C.: Machine learning for improvement of upper-tropospheric relative humidity in ERA5 weather model data, Atmos. Chem. Phys., 25, 2845–2861, https://doi.org/10.5194/acp-25-2845-2025, 2025.

Wong, H.-W. and Miake-Lye, R. C.: Parametric studies of contrail ice particle formation in jet regime using microphysical parcel modeling, Atmospheric Chemistry and Physics, 10, 3261–3272, https://doi.org/10.5194/acp-10-3261-2010, 2010.

Yu, F., and R. P. Turco, The role of ions in the formation and evolution of particles in aircraft plumes, Geophys. Res. Lett., 24, 1927-1930, 1997.

Yu, F., R. P. Turco, and B. Kärcher, The possible role of organics in the formation and evolution of ultrafine aircraft particles, J. Geophy. Res., 104, 4079-4087, 1999.

Yu, F., B. Kärcher, and B. E. Anderson, Revisiting contrail ice formation: Impact of primary soot particle sizes and contribution of volatile particles, Environmental Science & Technology, https://doi.org/10.1021/acs.est.4c04340, 2024.

Acknowledgements We thank the flight crews of the DLR Falcon and the Airbus A321neo for excellent flight operations. This work was supported by the DLR Aeronautics Research Programme within the Project NEOFUELS, and by the French VOLCAN programme funded by the Direction Générale de l'Aviation Civile (DGAC). C.V. and T.B. acknowledge funding by DFG by projects no 510826369 (ECOCON) and by the European Union's Horizon Europe program under grant no 101192301 (A4CLIMATE). F.Y. acknowledges funding support from the U.S. National Science Foundation (NSF) (AGS-2325458).

Author Contributions CV, CR, SK, and KS planned and coordinated the flight experiment; RM, DS, RD, SK, TB, TJW, LE, CH, EH, ML, AM, GM, AR, MS, PS and AG and performed the in-flight measurements and analysed the data; GLC, JM and ERE operated the A321neo and instruments; JZ and AR assisted on engine data interpretation, KS, GE and PLC analysed the fuel compositions; RM performed the contrail data evaluation, RD the aerosol and TB the trace gas analysis and AD performed the contrail forecast. FY, NB, MW applied the contrail models and performed model runs. C.V. wrote the paper. All authors contributed to the manuscript.

Author Information

CR, KS, GLC, JM and ERE are employed by Airbus; JZ is employed by General Electric, AR is employed by CFM Safran. All other authors declare that they have no conflict of interest.

Correspondence to Christiane.Voigt@dlr.de

Data availability

The datasets for this study are available in the data repository at https://halo-db.pa.op.dlr.de/.

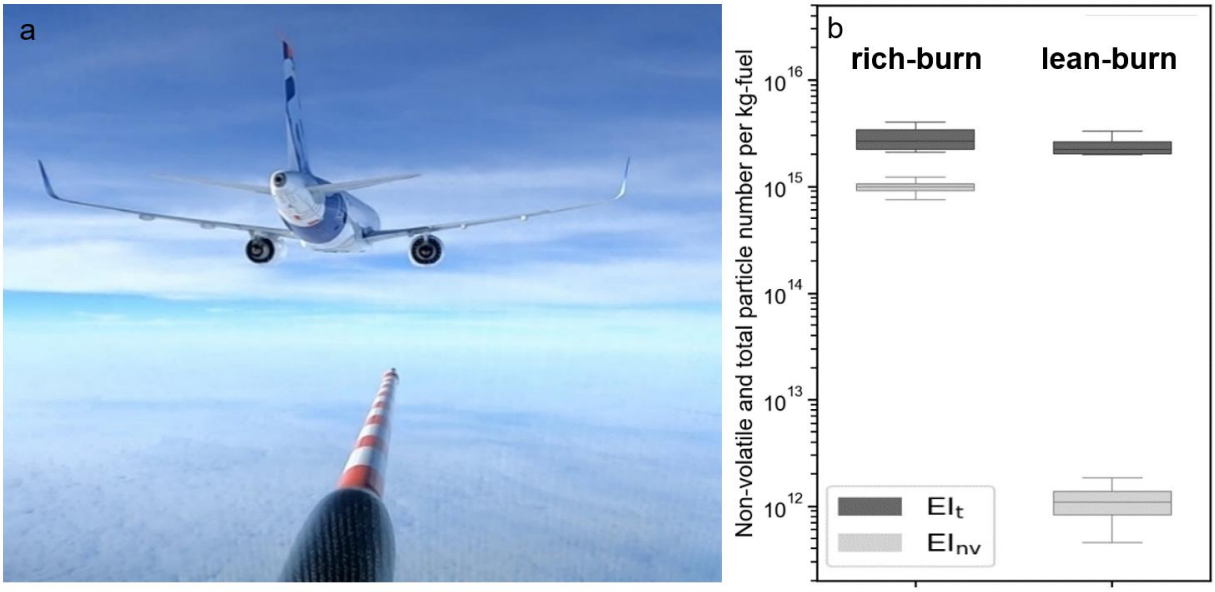

Figure 1 | a Noseboom of DLR's research aircraft Falcon chasing the Airbus A321neo equipped with CFM LEAP-1A lean-burn engines during an emission flight at a distance of 30 to 160 m and **| b Emission indices of total particles (EI_t, dark gray) and non-volatile particles (EI_{nv}, light gray) emitted per kg-fuel in forced rich-burn and lean-burn engine conditions for reference Jet A-1 fuel.** Median non-volatile and total particle number emissions indices (EI_{nv} with d > 14 nm, and EI_t with d > 5 nm), 25 and 75 percentiles, and minimum and maximum.

In the lean-burn mode, the non-volatile (i.e. soot) particle number emissions are reduced by more than 3 orders of magnitude compared to the forced rich-burn mode.

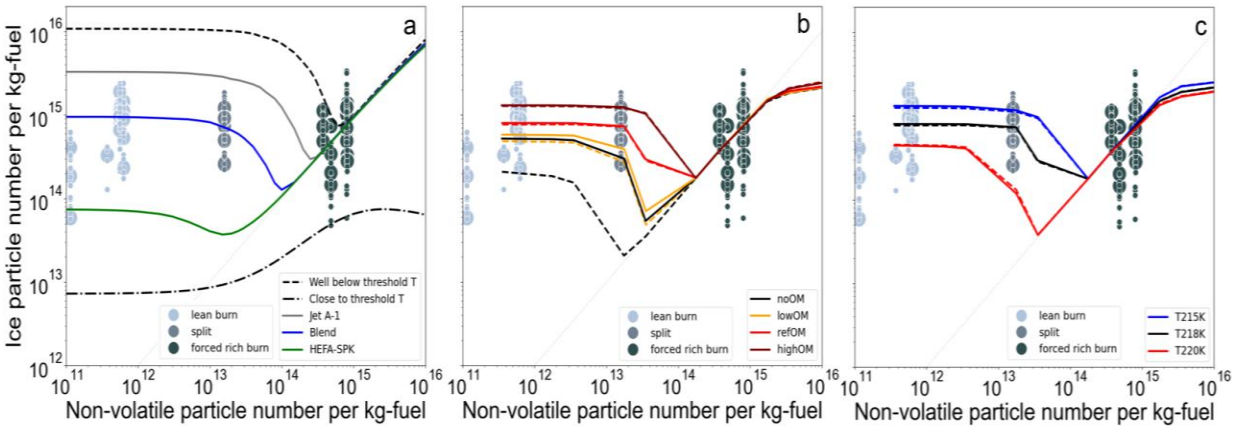

Figure 2 Correlation between the non-volatile (i.e. soot) particle number emission index (EI_{nv}) and the ice emission index (EI_{ice}) in lean-burn and forced rich-burn combustor conditions as well as for an intermediate fuel split point for all fuels (see Tables 1, 3, 4). Cruise measurement data are shown by symbols and model results by lines. Large (small) symbols show mean (individual) non-volatile (d > 14 nm), and ice (d > 0.6 µm) particle number emissions indices per kg-fuel binned in 1K temperature intervals. The settings and ambient conditions for the far-field contrail and the near-field emission measurements are given in the Supplement.

In order to fill the gap between rich and lean-burn combustor modes, an additional fuel distribution has been defined for this campaign, where the pilot flow was a bit increased and the main flow decreased compared to the normal lean-burn mode, shown here as intermediate split point.

Figure 2 | a Correlation between the non-volatile (i.e. soot) particle number emission index (EI_{nv}) and the ice emission index (EI_{ice}) The lines show results from the updated aerosol and contrail microphysics (ACM) model (Yu et al., 2024). Based on the observations, the simulations have been extended to 1×10^{11} soot particles kg^{-1}-fuel. For the present study, the ACM is improved by explicitly simulating the condensation of low volatile organic matter representing lube oil vapors (LOM) on volatile sulfate aerosol, assuming EI_{LOM} of 25 mg kg^{-1}-fuel and 195 (gray line), 41 (blue) and 3 (green) parts per million by mass of fuel sulfur content for temperatures close to 215 K, see Table 1. The upper and the lower lines indicate the theoretically expected soot and contrail ice crystal numbers for 500 ppmm fuel sulfur content and EI_{LOM} of 25 mg kg^{-1}-fuel at cold temperatures (dashed line) around 10 K below the contrail formation threshold temperature T_S (Schumann, 1996) and close to T_S, updated from Yu et al. (2024).

Figure 2 | b Correlation between the non-volatile (i.e. soot) particle number emission index (EI_{nv}) and the ice emission index (EI_{ice}), and model sensitivity ti the presence of organic matter. The lines show results from the updated contrail microphysical model (MoMie; Rojo et al., 2015) simulated for Jet A-1 (solid line) and HEFA (dashed line) with different fuel sulfur contents (195 and 3 parts per million by mass of fuel sulfur, respectively, see Table 1) for an average ambient temperature of 218 K; results are shown for no organic matter included (noOM, black lines) and for three different emission indices EI_{OM1} of the soluble organic compound OM1 with 5, 50 and 500 mg kg^{-1}-fuel, shown by yellow (lowOM), red (refOM), and dark-red (highOM) lines, respectively. In these simulations, the emission index of the insoluble organic compounds (OM2) EI_{OM2} is fixed to 15 mg kg^{-1}-fuel.

Figure 2 | c Correlation between the non-volatile (i.e. soot) particle number emission index (EI_{nv}) and the ice emission index (EI_{ice}), sensitivity for different temperatures

The lines show results from the contrail microphysics model (MoMie) from Rojo et al. (2015). Here, results for Jet A-1 (solid line) and HEFA (dashed line) with EI_{OM2} of 15 mg kg^{-1}-fuel (i.e. insoluble organic compounds) and reference EI_{OM1} of 50 mg kg^{-1}-fuel are simulated for three different temperatures of 215, 218 and 220 K. In the lean-burn mode, a strong dependence of EI_{ice} on ambient temperature is observed and modelled.

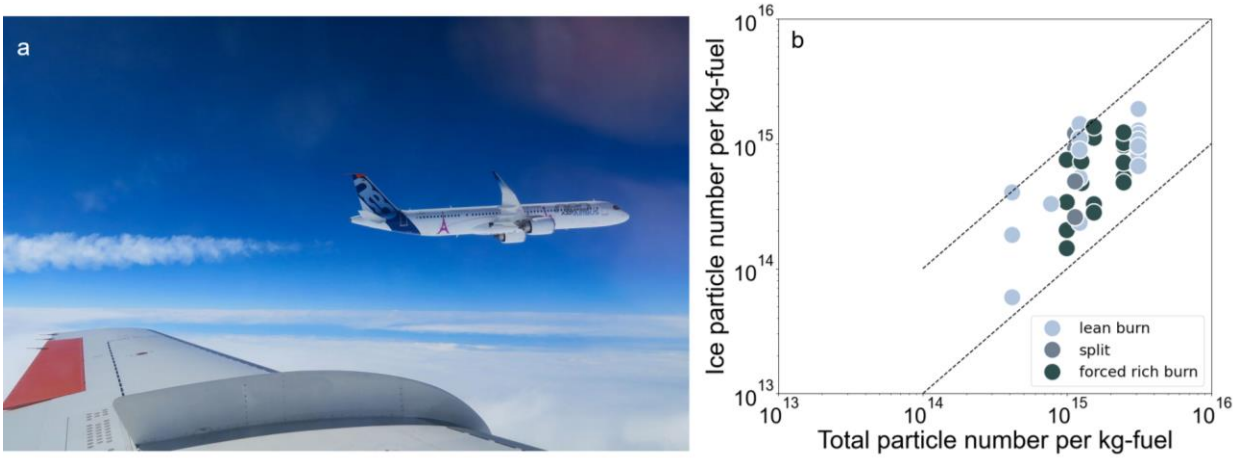

Figure 3 | a Foto of a contrail forming behind the A321neo taken from the research chase aircraft Falcon | b Correlation between measured total (i.e. volatile and non-volatile) particle emission indices (EI_t) and ice emission indices (EI_{ice}) per kg of burned fuel in forced rich-burn, lean-burn and fuel split point engine conditions for all fuels at ambient conditions given in Tables 1 to 3.

Symbols show mean total (d>5nm), and ice (>0.6 µm) particle emissions indices binned in 1K ambient temperature bins, see also Figure 2. The upper and lower dashed lines bound the measurement data and indicate the 1:1 and the 0.1:1 line. Emission measurements were taken in the near field and contrail measurements in the far field as given in Tables 2 and 3 and the methods.

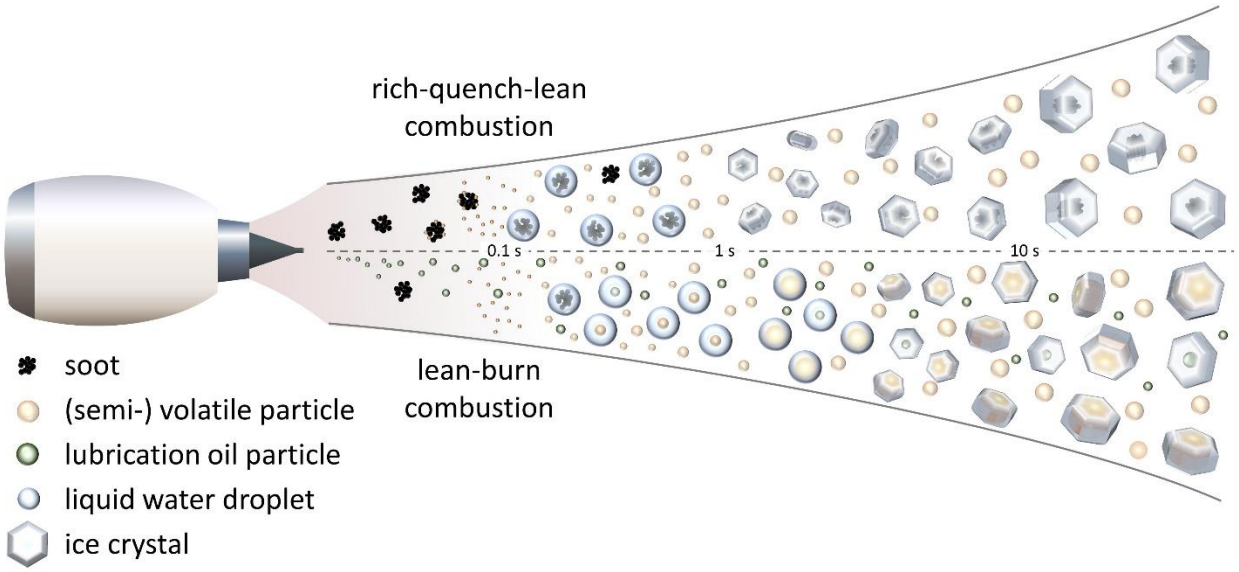

Figure 4 Sketch of the ice formation processes for current rich-quench-lean and lean-burn engine configurations

Rich-quench-lean combustor engines (top half) result in direct emissions of large numbers of soot particles. After around 0.1 s, the hot exhaust with gaseous volatile compounds have cooled enough to condense and form small volatile aerosol particles. Due to the Kelvin effect, the larger soot particles are activated to water droplets. After around 1s, the water droplets freeze homogeneously and the ice crystals and volatile particles continue to grow. During lean-burn combustion (bottom half), significantly less soot particles are emitted. For the tested lean-burn engine configuration, the oil venting system is located in the center of the core flow. Here, the venting of lubrication oil leads to the formation of oil vapors that condense on existing volatile and soot particles or nucleate new lubrication oil particles in the cooling exhaust. As these volatile aerosols grow, they can be activated to water droplets together with the low number of soot particles. The droplets subsequently freeze to form ice crystals which grow from uptake of exhaust and ambient water vapor.

Table 1

Fuel	Fuel components	Hydrogen content [%m/m]	Carbon content [%m/m]	Sulfur content [%m/m]	Aromatic content [%v/v]	Naphthalene content [%v/v]
Jet A-1	conv. Jet A-1	14.1	85.9	0.0195	12.8	0.6
HEFA-SPK	100% HEFA-SPK	15.3	84.7	0.00032	<1	<0.1
SPK+LA	HEFA-SPK + low aromatics	14.8	85.2	0.00019	8.4	<0.1
SPK+HA	HEFA-SPK + high aromatics	14.3	85.7	0.00005	17.6	<0.1
Blend	19% Jet A-1 + 81% HEFA-SPK	15.1	84.9	0.0041	2.5	0.2
Jet A-1	World average	13.9	85.1	0.0460	19.2	1.2

Table 1: **Composition of probed fuels and of average Jet A-1**. Fuel composition and properties for fuels used during NEOFUELS/VOLCAN; world average Jet A-1 composition from Hadaller et al. (2006)

METHODS

Source aircraft and engines

The A321neo Airbus A321neo-251NX (serial number 7877) was equipped with two CFM LEAP-1A engines. The CFM LEAP-1A35 turbofan engine has a maximum rated thrust of 143.1 kN, a maximum overall pressure ratio of 38.5 and a bypass ratio of 10.5 (ICAO EEDB). See Unique Identification Number 01P20CM135 for its emission certification data.

The CFM LEAP-1A features a lean-burn combustor or staged combustor with a rich-burn pilot stage and a lean-burn main stage (Stickles and Barret, 2013). The lean-burn mode is operated during take-off, climb and cruise phases. Both the central pilot injector and the annular main injector ring inject fuel into the combustion chamber, resulting in wide areas of lean fuel-to-air ratios and a more homogeneous temperature distribution in the combustor. The annular main injector is switched off for descent and taxi phases (rich-burn mode) to avoid engine instability. Operating conditions typical for cruise were selected for the flight tests and the T30 temperature at the combustor inlet was fixed for the different measurement points to allow comparability between lean-burn and rich-burn conditions. As the combustor operates normally in lean-burn conditions in cruise, this also implies that the rich-burn mode had to be forced by engine FADEC adjustments.

Falcon Instrumentation

Contrail ice particles, aerosols, and trace gases were measured with a set of well characterized instruments that have been deployed aboard aircraft in previous campaigns (e.g. Voigt et al., 2010; Voigt et al., 2021; Voigt et al., 2022; Dischl et al., 2024; Märkl et at., 2024). Temperature and other meteorological data were measured with the meteorological measurement system on Falcon (Giez et al., 2017). In the following, we describe the instruments and data evaluation used for this study in more detail.

Contrail ice particle instrument

Contrail ice particles in the size range between 0.6 and 50 µm diameter were measured with the Cloud and Aerosol Spectrometer (CAS) (Baumgardner et al., 2001; Voigt et al., 2017), mounted in the inner left underwing pylon of the DLR Falcon. When the Falcon aircraft flies through contrails, ice particles pass through the instrument and scatter light from a laser beam (λ = 658 nm) in a sample area of 0.22 ± 0.04 mm^2. By detection of the scattered light intensity, ice particle number concentrations as well as particle size distributions can be determined using Mie scattering theory (Mie, 1908) and following the calibration method of Rosenberg et al. (2012). Ice particle number concentrations are corrected for coincidence effects using an empirically derived correction function described in Märkl et al. (2024). Shattering effects (Field et al., 2003; Baumgardner et al., 2017) were not observed and therefore no correction was performed. The overall ice particle number concentration uncertainty is determined by uncertainties from the use of total air speed (TAS) for the sample air speed (SAS), by the sample area uncertainty, and by the concentration dependent counting uncertainty. This amounts to an overall ice particle number concentration uncertainty of ±20% for the presented measurements.

Aerosol instruments

Total and non-volatile particle number concentrations were measured using condensation particle counters (CPC) TSI models 3010 and 3768a (TSI Inc, Minneapolis, MN, USA), which are modified and optimized for airborne applications. The CPCs show different lower size cut-offs of 5 nm diameter for total particles and 14 nm diameter for non-volatile particles. Aerosol instruments retrieved the sample air through a forward-facing, near-isokinetic inlet. To determine non-volatile particle concentrations, three CPCs were operated behind a heated inlet line of a thermal denuder at 250°C removing volatile components. The sample flow could be diluted by a factor of 30 using

an inline dilution system to prevent saturation of the particle counters. CPC data were corrected for reduced detection efficiencies at low pressures and for particle losses in the thermodenuder. The mean uncertainty in particle number concentrations is estimated at ±10% (Dischl et al., 2024).

CO_2, NOx, and H_2O instruments and meteorological measurement system

Carbon dioxide (CO_2) was measured using a high frequency (10 Hz) non-dispersive infrared gas analyser (LI-7000, LI-COR biosciences) aboard the Falcon. Additionally, a specifically adapted cavity ring down spectrometer G2401-m (Picarro Inc., Santa Clara, CA, USA), well known for its stable instrument performance, was used to monitor and cross-check CO_2 background values. The sample air was passed to both instruments via backward facing inlets mounted to the upper part of the fuselage of the Falcon. The LI-7000 was modified in-house for aircraft deployment and makes use of the absorption of infrared radiation by CO_2 molecules inside a measurement cell. By comparing the signal with that from a reference cell containing zero air, the absolute absorption and CO_2 mixing ratio is derived. An occurring temperature drift of the instrument with time is compensated for by frequent zero measurements every 30 min during the flight. In the post-processing, the CO_2 mixing ratio is corrected for water vapor dilution in order to report dry-air mole fractions. The accuracy of the LI-7000 CO_2 measurement is 0.2 ppm, thereby taking account of the reproducibility of the calibration standards (0.18 ppm) (using NOAA standards traceable to the WMO CO_2 calibration scale), the precision (0.08 ppm) and the uncertainty of water vapor dilution correction (0.1 ppm), for more details see Harlass et al. (2024).

Reactive nitrogen (NOy) was measured using a chemiluminescence detector (CLD TR 780, ECO PHYSICS AG, Switzerland). The chemiluminescence technique is a well-established method. Using a heated gold converter (T=290°C) with hydrogen (H_2) as a reducing agent, reactive nitrogen species NOy (NO+NO2+HNO3+PAN and others) are converted to NO molecules, which are subsequently going through the chemiluminescence reaction with O3. Due to the instrument's measurement range up to 1000 ppb, a dilution system was integrated in order to measure higher concentrations in the exhaust plumes. Thereby, zero air was added to the sample air at a ratio of 1:4 prior to the measurement. The detection limit of the CLD TR 780 is 0.55 ppb at a time resolution of 1 Hz (Harlass et al., 2024).

Water vapor mixing ratios (H_2O) were measured with the water vapor mass spectrometer AIMS-H2O (Kaufmann et al. (2016), Kaufmann et al. (2018)) with a frequency of 2.5 Hz sampling air

through a backward facing inlet at the upper fuselage of the Falcon. From water vapor mixing ratio in combination with static air temperature and static pressure measurements, we can derive the relative humidity over ice (RHi), which is the relevant parameter for contrail persistence. For this calculation, the ice saturation pressure formulation from Eq. 7 in Murphy and Koop (2005) was used. The uncertainty in RHi is estimated to be around 15% by error propagation of uncertainty in water vapor mixing ratio (8% to 12% relative) and temperature (0.5K). Uncertainty in static pressure has only a minor contribution to the RHi uncertainty.

Meteorological Data Set The aircraft is equipped with a basic instrumentation which measures pressure, temperature, air flow, wind speed and humidity at data rates of up to 100Hz. The quality of the measurement depends not only on a proper lab calibration of the sensors but also on an accurate parameterization of the aerodynamic effects in the vicinity of the aircraft fuselage (Wendisch and Bregnuier, 2013). These effects were determined by in flight calibration methods including the trailing cone method and maneuvers (Boegel and Baumann, 1991).

The NEOFUELS/VOLCAN campaign

15 flights were performed with the Falcon behind the A321neo over the Atlantic and the Mediterranean in March 2023. For the six emission flights, the A321neo and the DLR Falcon entered a two-aircraft formation with constant air speed of 0.59 Mach at an altitude of 9 to 10 km. Starting at a close distance of about 30 m to the right-hand engine of the leading aircraft, the Falcon repeatedly entered its emission plume from below, acquiring plume emission data for 45 seconds followed by a 30-second sequence of background data, with 5 repetitions at the same engine setting to obtain good data statistics. As the Falcon was pushed back by the exhaust plume during the sampling sequences, the Falcon's distance from the engine exit plane increased. To avoid entrainment of the wing-tip vortices, the Falcon descended below the plume at about 160 m distance and increased speed to catch up with the Airbus. This measurement sequence was repeated several times under different engine conditions or for different fuels. Contrails are not yet fully developed at these close distances and we probed contrails in the far field at distances of 6 to 29 km behind the Airbus aircraft flying at a mean typical cruise speed of 0.78 Mach with both engines operating at the same power and combustor settings.

Engine emission measurements and evaluation

A time series of data collected by the DLR Falcon during a near-field emission measurements flight on 7 March 2023 is shown in Figure M1. A321neo plume encounters are evident by repeated sequences with large enhancements in total particles, CO_2 and NO_y concentrations, and temperatures above background levels. Smaller fluctuations in the flight altitude indicate direct pilot manoeuvres in the exhaust plume with the auto-pilot switched off. Here, the pilots split aircraft control, where one steered and kept the Falcon in the exhaust while the other operated the thrust. A sequence of five plume encounters at the same engine power and combustor settings is followed by a few minutes break to measure ambient conditions and to allow the change of engine power settings with respect to T30 combustor inlet temperature, combustion mode, or fuel. Several orders of magnitude enhancements in total particle concentrations > 5 nm are measured in all plume sequences, while distinct different features are observed in the non-volatile particles. Similar to total particles, large peaks are observed in non-volatile particle concentrations in the exhaust in the forced rich-burn mode, while non-volatile particle concentrations are close to background levels in the lean-burn combustion mode at similar T30 combustor inlet temperature settings.

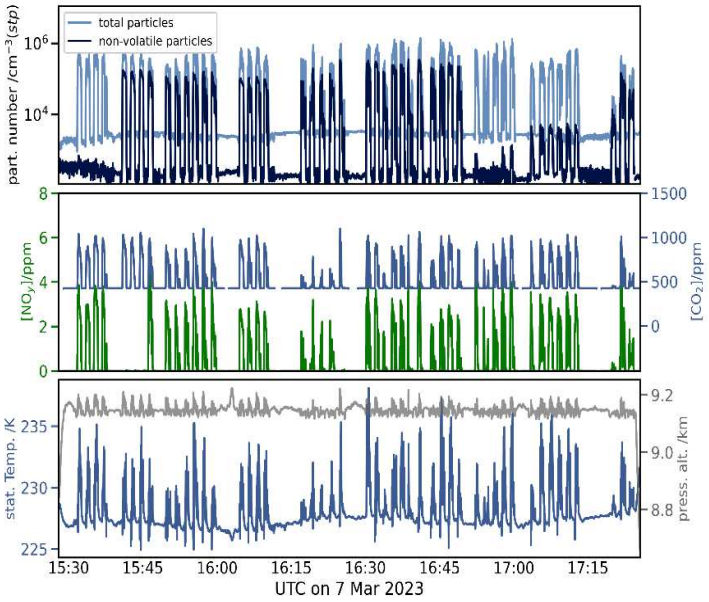

Figure M1 | Time series of 1-Hz data measured in the A321neo emission plume during forced rich-burn and lean-burn measurement sequences.

Number concentration of non-volatile particles larger than 14 nm (i.e. soot, dark blue line) and of total particles larger than 5 nm (i.e. volatile and non-volatile particles, light blue line) in cm^{-3} at standard pressure, CO_2 (blue) and NO_y (green) mixing ratio in parts per million by volume, temperature (blue) in Kelvin and pressure altitude (light gray) in kilometres. Measurements were taken at less than 3 sec plume age at distances between 30 and 160 m. Measurements at lean-burn mode are visual by low soot particle concentrations, e.g. between 15:30 and 15:40 UTC or between 16:50 and 17:00 UTC. Also, the intermediate fuel split point with slightly enhanced non-volatile particles is indicated between 17:03 and 17:13 UTC.

Calculation of emissions indices

To conduct valid comparisons of particle number concentrations independent of dilution level, particle number concentration enhancements ΔX need to be compared to mixing ratio enhancements of a tracer such as CO_2 (ΔCO_2). By assuming homogeneous mixing of particles and trace gases, the resulting ratio $\Delta X/\Delta CO_2$ serves to gauge the level of plume/contrail dilution. The amount of emitted CO_2 per mass of burned fuel is a fuel property, depending on the ratio of hydrogen to carbon atoms in the fuel, and is described by the CO_2 emission index EI_{CO2} (Moore et al., 2017). With the ratio of molar mass of air (M_{air}) to molar mass of CO_2 (M_{CO2}) and density of air (ρ_{air}), an emission index for species X can be calculated (Beyersdorf et al., 2014)

$$EI_x = \left(\frac{\Delta X}{\Delta CO_2}\right) \cdot \left(\frac{M_{air}}{M_{CO_2} \cdot \rho_{air}}\right) \cdot EI_{CO2}$$

Here, density of air and particle concentration enhancement ΔX are given at standard temperature and pressure (STP) for the aerosol measurements and at ambient conditions for ice particle measurements. For non-volatile and total particles, EI_x describes the number of emitted particles per mass of fuel burned, EI_{nv} that of non-volatile particles, and EI_t that of total particles including volatiles and non-volatiles. Ice particles, on the other hand, form on emitted aerosols and are not directly emitted and are labelled EI_{ice} for consistency with EI_{nv} and EI_t. The ambient and engine conditions for the EI_{nv} and EI_t shown in Fig. 1b are given below.

Table 2

	Lean-burn	Forced Rich-burn
Plume age (s)	2	2-3

Sampling time (s)	215	850
Ambient RHi (%)	68-90	40-86
Ambient T (K)	229-231	228-232
Delta T_SA (K)	0.5-1	0.5-2
Altitude of source aircraft (m)	9140	9140
Speed of source aircraft (Mach)	0.59	0.59
Median EI_nvPM (kg^{-1}-fuel) Median Range	 1.0×10^{12} $(0.5\text{-}1.9)\times10^{12}$	 1.0×10^{15} $(0.8\text{-}1.1)\times10^{15}$
Median EI_t (kg^{-1}-fuel) Median Range	 2.1×10^{15} $(2.0\text{-}3.3)\times10^{15}$	 2.7×10^{15} $(2.1\text{-}4.0)\times10^{15}$

Table 2: Ambient and engine conditions and particle emission indices for data for Fig. 1b

Contrail emission indices and measurement conditions

Contrail encounters are only evaluated where ice particle and trace gas measurements are conducted approximately homogeneously. Therefore, correlations of ice particle concentration and CO_2 mixing ratio time series are calculated and contrail encounters are rejected if the resulting correlation is lower than 0.6, similar to the method employed in Märkl et al. (2024). Uncertainties in aerosol/ice particle measurement, CO_2 and aerosol particle background determination, CO_2 measurement, and ambient condition measurements are propagated to determine an EI uncertainty for every plume/contrail encounter. This results in an average EI_{nv} and EI_t uncertainty of 10±5 % and an average EI_{ice} uncertainty of 38±16 %.

In contrast to emission measurements performed in ice-free conditions at distances up to 160 m, contrail ice particles are probed at larger distances of 6 km to 29 km. At those distances, the contrail is in a relatively stable state if ambient conditions are supersaturated with respect to ice so that valid comparisons of combustion modes can be performed. Contrail ages are determined from the GPS positions of the two aircraft and using wind field measurements onboard the preceding aircraft to determine contrail drift as described in Märkl et al. (2024). Ambient conditions, as well as fuel properties, and an assumed overall propulsion efficiency of 0.36 (Epstein, 2014) enable calculation of the Schmidt-Appleman contrail formation threshold T_{SA} (Schumann, 1996). The

difference of ambient temperature to the formation threshold ΔT_{SA} ranged between -4.5 and -19.0 K for the shown contrail encounters. Table 3 shows the engine and ambient conditions for contrail data shown in Figures 2 and 3. As volatile and non-volatile particle emission data during the contrail sampling events could have been spoiled by the presence of contrail ice crystals, the engine particle emission data for Figures 2 and 3 were taken from near-field emission measurements at the same engine conditions in terms of engine inlet temperature T30, and the same fuels, see Table 4. Different engine conditions also explain lower EI_{nv} for Jet A-1 compared to engine emission data shown in Table 2.

Table 3

Combustion mode	Lean-burn	Split	Forced Rich-burn
Contrail age (s)	29-117	36-65	24-122
Sampling time (s)	1503	590	2490
Ambient RHi (%)	100-180	100-123	100-143
Ambient T (K)	212-226	216-219	211-223
Delta T_SA (K)	-4.5 - -13.9	-7.9 - -12.5	-5.5 - -14.9
Altitude of source aircraft (m)	9199-11488	9646-10608	9422-11490
Speed of source aircraft (Mach)	0.747-0.794	0.745-0.792	0.641-0.798

Table 3: **Ambient conditions for the contrail data (Fig. 2 and 3)** Measurement conditions in contrails were filtered for 100% RHi, >60% correlation of ice particle concentration and tracer, <100% uncertainty, and stable engine conditions, see also methods for further explanations.

Table 4

	Lean-burn	Split	Forced Rich-burn
Plume age (s)	2-3	3	2-3
Sampling time (s)	1828	343	1811
Ambient RHi (%)	40-80	60-80	40-80
Ambient T (K)	228-235	228-231	228-235
Delta T_SA (K)	0.5 - 5	0.5	0.5 - 5
Altitude of source aircraft (m)	8830-9140	9140	8830-9140
Speed of source aircraft (Mach)	0.59	0.59	0.59

EI_nvPM (kg^{-1}-fuel)			
Median	4.6×10^{11}	1.6×10^{13}	8.5×10^{14}
Range	$(1.1\text{-}6.3) \times 10^{11}$		$(3.8\text{-}8.2) \times 10^{14}$
EI_t (kg^{-1}-fuel)			
Median	1.3×10^{15}	1.1×10^{15}	1.5×10^{15}
Range	$(0.4\text{-}3.1) \times 10^{15}$		$(1.0\text{-}2.5) \times 10^{15}$

Table 4: **Ambient and engine conditions for emission data related to contrail data at the same engine conditions (Fig. 2 and Fig. 3)** As volatile and non-volatile particle emission data during the contrail sampling events could have been spoiled by the presence of contrail ice crystals, the particle emission data for Figures 2 and 3 were taken from near-field emission measurements at the same engine settings in terms of engine inlet temperature T30, see methods.

Models

The Aerosol and Contrail Microphysics (ACM) model

An aerosol and contrail microphysics (ACM) model, as detailed in Yu et al. (2024), is employed and improved for this study. The ACM model is a parcel model of jet plume aerosol and ice microphysics developed in the late 1990s (Yu and Turco, 1997, 1998; Yu et al., 1999), with the volatile particle formation module improved with algorithms and thermodynamic data developed in the past two decades, and the contrail microphysics module improved with a new soot activation scheme (Yu et al., 2024). The ACM model captures the dependence of contrail ice particles formed on emitted non-volatile soot particles and can explain less-than-unity fractions of soot particles forming contrail ice particles (Yu et al., 2024) as recently observed during ECLIF campaigns (Voigt et al., 2021, Märkl et al., 2024). More importantly, previous ACM model simulations have predicted that, because of the activation of volatile particles, the number of contrail ice particles formed when soot emission is very low (i.e., in soot-poor regime) can be comparable to that of soot-rich regime (Kärcher and Yu, 2009; Kärcher, 2018; Yu et al., 2024). More details of the ACM model can be found in Yu et al. (2024). For the present study, the ACM is improved by explicitly simulating the condensation of low volatile lube oil vapor (LOM) on sulfate aerosol, assuming an EI_{LOM} of 25 mg kg^{-1}-fuel and 195, 41 and 3 parts per million by mass of fuel sulfur as given in Table 1.

The Modèle Microphysique pour Effluents (MoMiE) contrail model

The Modèle Microphysique pour Effluents (MoMiE) is a microphysical model first developed at ONERA by Sorokin et al. (2001) and Vancassel et al. (2010) for typical kerosene fuels, and then

adapted to simulate the combustion of SAF by Rojo et al. (2015). The model accounts for two processes, heterogeneous nucleation on soot particles and homogeneous nucleation of volatile particles composed of sulfur and organic species (Wilemski et al. 1995). Two types of organic species are distinguished in the model: organic compounds that are soluble in water (OM1), which can nucleate to form a new volatile aerosol distribution, and organic compounds considered insoluble in water (OM2), which are able to condense on soot particles (Turpin et al. 2000). Processes of coagulation, condensation and freezing are included in the model (Jacobson et al. 1994; Pruppacher et al. 1997), as well as the effects of ion recombination, which are simulated by considering positive organic clusters and negative sulfates (Arnold et al. 2000). All particle distributions are discretized in size bins. Plume dilution is calculated with the analytic formula by Schumann et al. (2002).

Different simulations have been computed to cover initial soot particle number emission indices in the range emitted by lean-burn and rich-burn combustors and to account for the two fuel types Jet A-1 and HEFA. In all simulations, soot particles are represented by a log-normal distribution with 35 nm median diameter and a standard deviation of 1.6. Jet A-1 and HEFA cases are distinguished in the simulations with different fuel sulfur contents (195 and 3.2 parts per million by mass of fuel sulfur, based on Table 1) simulated for an average ambient temperature 218 K. The model (noOM, for no organic matter), also accounts for the sensitivity of both fuel types to the presence of organics and to the variability of the initial amounts of soluble organic compounds OM1. The MoMie model is sensitive to changes in ambient temperature for the two fuel types. Simulations first indicate that EI_{ice} is particularly sensitive to temperature and organic matter in the low-soot regime. Increasing the fraction of organics at emission increases contrail ice crystal numbers by one order of magnitude and decreasing the ambient temperature by two Kelvin doubles the number of ice crystals. The high variability in the observations compared to the results of both models confirms the impact of temperature and fuel sulfur content on contrail ice crystals. It also suggests that other factors and additional species like organics and lubrication oils could play a role as condensation nuclei.

References (Methods)

Arnold F., Kiendler A., Wiedemer V., Aberle S., Stilp T., Busen R.: Chemiion concentration measurements in jet engine exhaust at the ground: implications for ion chemistry and aerosol formation in the wake of a jet aircraft. Geophys Res Lett, 27:1723–6, https://doi.org/10.1029/1999GL011096, 2000.

Baumgardner, D., Jonsson, H., Dawson, W., O'Connor, D., and Newton, R.: The cloud, aerosol and precipitation spectrometer: a new instrument for cloud investigations, Atmos Res, 59-60, 251–264, https://doi.org/10.1016/S0169-8095(01)00119-3, 2001.

Baumgardner, D., Abel, S. J., Axisa, D., Cotton, R., Crosier, J., Field, P., Gurganus, C., Heymsfield, A., Korolev, A., Krämer, M., Lawson, P., McFarquhar, G., Ulanowski, Z., and Um, J.: Cloud Ice Properties: In Situ Measurement Challenges, Meteor Mon, 58, 91–923, https://doi.org/10.1175/amsmonographs-d-16-0011.1, 2017.

Boegel, W., and R. Baumann:Test and Calibration of the DLR Falcon Wind Measuring System by Maneuvers. J. Atmos. Oceanic Technol., 8 (1), 5, 18, http://dx.doi.org/10.1175/1520-0426, 1991.

Borrmann, S., Luo, B., and Mishchenko, M.: Application of the T-matrix method to the measurement of aspherical (ellipsoidal) particles with forward scattering optical particle countersApplication of the T-matrix method to the measurement of aspherical (ellipsoidal) particles with forward scattering optical particle counters, J Aerosol Sci, 31, 789–799, https://doi.org/10.1016/S0021-8502(99)00563-7, 2000.

Giez, A., Mallaun, C., Zöger, M., Dörnbrack, A., and Schumann, U.: Static Pressure from Aircraft Trailing-Cone Measurements and Numerical Weather-Prediction Analysis, Journal of Aircraft, 54, 1728–1737, https://doi.org/10.2514/1.C034084, 2017.

Harlass, T., Dischl, R., Kaufmann, S., Märkl, R., Sauer, D., Scheibe, M., Stock, P., Bräuer, T., Dörnbrack, A., Roiger, A., Schlager, H., Schumann, U., Pühl, M., Schripp, T., Grein, T., Bondorf, L., Renard, C., Gauthier, M., Johnson, M., Luff, D., Madden, P., Swann, P., Ahrens, D., Sallinen, R., and Voigt, C.: Measurement report: In-flight and ground-based measurements of nitrogen oxide emissions from latest-generation jet engines and 100 % sustainable aviation fuel, Atmos. Chem. Phys., 24, 11807–11822, https://doi.org/10.5194/acp-24-11807-2024, 2024.

Heymsfield, A., D. Baumgardner, P. DeMott, P. Forster, K. Gierens, and B. Kärcher: Contrail Microphysics. Bull. Amer. Meteor. Soc., 91, 465–472, https://doi.org/10.1175/2009BAMS2839.1, 2010.

ICAO EEDBv30, ICAO Engine Emissions Data Bank, Version30, 7/2024, last accessed 20250429, https://www.easa.europa.eu/en/domains/environment/icao-aircraft-engine-emissions-databank, 2025.

Lance, S.: Coincidence errors in a Cloud Droplet Probe (CDP) and a Cloud and Aerosol Spectrometer (CAS), and the improved performance of a modified CDP. *Journal of Atmospheric and Oceanic Technology* 29(10), 1532–1541, 2012.

Field, P. R., Wood, R., Brown, P. R. A., Kaye, P. H., Hirst, E., Greenaway, R., & Smith, J. A.: Ice particle interarrival times measured with a fast FSSP. Journal of Atmospheric and Oceanic Technology, 20(2), 249–261, 2013.

Jacobson M.Z., Turco R.P., Jensen E.J., Toon O.B., Modeling coagulation among particles of different composition and size, Atmos. Environ., Vol. 28, pp. 1327-1337, https://doi.org/10.1016/1352-2310(94)90280-1, 1994.

Kaufmann, S., Voigt, C., Jurkat, T., Thornberry, T., Fahey, D. W., Gao, R.-S., Schlage, R., Schäuble, D., and Zöger, M.: The airborne mass spectrometer AIMS – Part 1: AIMS-H2O for UTLS water vapor measurements, Atmos. Meas. Tech., 9, 939–953, https://doi.org/10.5194/amt-9-939-2016, 2016.

Kaufmann, S., Voigt, C., Heller, R., Jurkat-Witschas, T., Krämer, M., Rolf, C., Zöger, M., Giez, A., Buchholz, B., Ebert, V., Thornberry, T., and Schumann, U.: Intercomparison of midlatitude tropospheric and lower-stratospheric

water vapor measurements and comparison to ECMWF humidity data, Atmos. Chem. Phys., 18, 16729–16745, https://doi.org/10.5194/acp-18-16729- 2018, 2018.

Märkl, R., PhD thesis, doi:10.25358/openscience-11418, 10.25358/openscience-11418, https://openscience.ub.uni-mainz.de/handle/20.500.12030/11439, 2025.

Pruppacher, H. R., Klett, J. D., & Wang, P. K. Microphysics of Clouds and Precipitation. Aerosol Science and Technology, 28(4), 381–382, https://doi.org/10.1080/02786829808965531, 1998.

Rosenberg, P. D., Dean, A. R., Williams, P. I., Dorsey, J. R., Minikin, A., Pickering, M. A., and Petzold, A.: Particle sizing calibration with refractive index correction for light scattering optical particle counters and impacts upon PCASP and CDP data collected during the Fennec campaign, Atmos Meas Tech, 5, 1147–1163, https://doi.org/10.5194/amt-5-1147-2012, 2012.

Sorokin A., Vancassel X., Mirabel P., On volatile particle formation in aircraft exhaust plume, Phys. Chem. Earth (C), Vol. 26, pp. 557-561, https://doi.org/10.1016/S1464-1917(01)00047-2, 2001.

Turpin B. J., Saxena P., Andrews E., Measuring and simulating particulate organics in the atmosphere: problems and prospects, Atmospheric Environment, Volume 34, Issue 18, Pages 2983-3013, ISSN 1352-2310, https://doi.org/10.1016/S1352-2310(99)00501-4, 2000.

Vancassel, X.P., Garnier, F.A. and Mirabel, P.J., In Plume Physics and Chemistry. In Encyclopedia of Aerospace Engineering (eds R. Blockley and W. Shyy), https://doi.org/10.1002/9780470686652.eae351, 2010.

Voigt, C., Schumann, U., Jurkat, T., Schäuble, D., Schlager, H., Petzold, A., Gayet, J.-F., Krämer, M., Schneider, J., Borrmann, S., Schmale, J., Jessberger, P., Hamburger, T., Lichtenstern, M., Scheibe, M., Gourbeyre, C., Meyer, J., Kübbeler, M., Frey, W., Kalesse, H., Butler, T., Lawrence, M. G., Holzäpfel, F., Arnold, F., Wendisch, M., Döpelheuer, A., Gottschaldt, K., Baumann, R., Zöger, M., Sölch, I., Rautenhaus, M., and Dörnbrack, A.: In-situ observations of young contrails – overview and selected results from the CONCERT campaign, Atmospheric Chemistry and Physics, 10, 9039–9056, https://doi.org/10.5194/acp-10-9039-2010, 2010.

Voigt, C., Schumann, U., Minikin, A., Abdelmonem, A., Afchine, A., Borrmann, S., Boettcher, M., Buchholz, B., Bugliaro, L., Costa, A., Curtius, J., Dollner, M., Dörnbrack, A., Dreiling, V., Ebert, V., Ehrlich, A., Fix, A., Forster, L., Frank, F., Fütterer, D., Giez, A., Graf, K., Grooß, J.-U., Groß, S., Heimerl, K., Heinold, B., Hüneke, T., Järvinen, E., Jurkat, T., Kaufmann, S., Kenntner, M., Klingebiel, M., Klimach, T., Kohl, R., Krämer, M., Krisna, T. C., Luebke, A., Mayer, B., Mertes, S., Molleker, S., Petzold, A., Pfeilsticker, K., Port, M., Rapp, M., Reutter, P., Rolf, C., Rose, D., Sauer, D., Schäfler, A., Schlage, R., Schnaiter, M., Schneider, J., Spelten, N., Spichtinger, P., Stock, P., Walser, A., Weigel, R., Weinzierl, B., Wendisch, M., Werner, F., Wernli, H., Wirth, M., Zahn, A., Ziereis, H., and Zöger, M.: ML-CIRRUS: The Airborne Experiment on Natural Cirrus and Contrail Cirrus with the High-Altitude Long-Range Research Aircraft HALO, Bull Am Meteorol Soc, 98, 271–288, https://doi.org/10.1175/BAMS-D-15-00213.1, 2017.

Wendisch, M. and Brenguier, J.-L.: Airborne Measurements for Environmental Research – Methods and Instruments, Wiley–VCH Verlag GmbH & Co. KGaA, Weinheim, Germany, Weinheim, Germany, https://doi.org/10.1002/9783527653218, ISBN: 978-3-527-40996-9, 2013.

Wilemski G., Wyslouzil B. E., Binary nucleation kinetics. I. Self-consistent size distribution. J. Chem. Phys, 103 (3), 1127–1136, https://doi.org/10.1063/1.469823, 1995.

Yu, F., and R. P. Turco, Contrail formation and impacts on aerosol properties in aircraft plumes: Effects of fuel sulfur content, Geophys. Res. Lett., 25, 313-316, 1998.